

RESEARCH ARTICLE

10.1002/2017JA025021

Key Points:

- The paper presents the statistical study of MSTIDs in equatorial latitudes over south-southeast of Brazil
- The propagation direction of MSTIDs changes according to the seasons
- The MSTIDs can be originated by gravity waves that propagate from the lower atmosphere

Supporting Information:

- Supporting Information S1
- Movie S1

Correspondence to:

C. A. O. B. Figueiredo,
cosme.figueiredo@inpe.br

Citation:

Figueiredo, C. A. O. B., Takahashi, H., Wrasse, C. M., Otsuka, Y., Shiokawa, K., & Barros, D. (2018). Medium-scale traveling ionospheric disturbances observed by detrended total electron content maps over Brazil. *Journal of Geophysical Research: Space Physics*, 123, 2215–2227. <https://doi.org/10.1002/2017JA025021>







Received 20 NOV 2017

Accepted 27 FEB 2018

Accepted article online 5 MAR 2018

Published online 14 MAR 2018

Medium-Scale Traveling Ionospheric Disturbances Observed by Detrended Total Electron Content Maps Over Brazil

C. A. O. B. Figueiredo¹ , H. Takahashi¹ , C. M. Wrasse¹ , Y. Otsuka² , K. Shiokawa² , and D. Barros¹ 

¹Instituto Nacional de Pesquisas Espaciais, São José dos Campos, Brazil, ²Institute for Space-Earth Environmental Research, Nagoya University, Nagoya, Japan

Abstract A ground-based network of Global Navigation Satellite Systems receivers has been used to monitor medium-scale traveling ionospheric disturbances (MSTIDs). MSTIDs were studied using total electron content perturbation maps and keograms over south-southeast of Brazil during the period from December 2012 to February 2016. In total, 826 MSTIDs were observed mainly in daytime, thus presenting median values of horizontal wavelength, period, and horizontal phase velocity of 452 ± 107 km, 24 ± 4 min, and 323 ± 81 m/s, respectively. The direction of propagation varies on the season: during the winter (June–August), the waves preferentially propagated to north-northeast, while in the other seasons the waves propagated to other directions. The anisotropy observed in the MSTID propagation direction could be associated with the region of the gravity wave generation that takes place in the troposphere. We also found that the MSTIDs were observed most frequently during the daytime, between 11 and 15 local time in winter and near to dusk solar terminator (17–19 local time) in the other seasons. Furthermore, the occurrence of MSTIDs was higher in winter. We suggest that atmospheric gravity waves in the thermosphere, mesosphere, and troposphere could play an important role in generating the MSTIDs and the propagation direction may depend on location of the wave sources.

1. Introduction

The traveling ionospheric disturbances (TIDs) are oscillations that occur in the ionospheric plasma, with the wavelengths having a range of hundreds to thousands kilometers and velocity of the order of hundreds of meters per second (Hunsucker, 1982; Kelley, 2011). Hunsucker (1982) has classified the TIDs with wavelengths of 100 to 1,000 km and period below 60 min as medium-scale TIDs (MSTIDs), although recent observations included MSTIDs with horizontal wavelengths up to 1,500 km (Otsuka et al., 2013).

The first observation of the TIDs has been dated in the 1940s (Munro, 1948). The phenomenon began to be modeled numerically in the 1950s (Hines, 1960). Since then, the TIDs have been studied through a variety of equipment such as ionosondes (Amorim et al., 2011; MacDougall et al., 2011; Munro, 1948), satellites beacon (Forbes et al., 2016; Garcia et al., 2016; Park et al., 2015), airglow imagers (Paulino et al., 2016; Pimenta et al., 2008), and the Global Navigation Satellite Systems (GNSS) (Otsuka et al., 2013; Saito et al., 1998).

The most of the studies on MSTIDs are concentrated in the northern hemisphere (NH) midlatitudes (Hernandez-Pajares et al., 2006, 2012; Kotake et al., 2007; Otsuka et al., 2011, 2013; Takeo et al., 2017; Tsugawa et al., 2007). These authors observed daytime MSTIDs propagating equatorward in the winter, while in the equinoxes and summer the MSTIDs propagate to southeastward, on the other hand, nighttime MSTIDs propagating southwestward. The different direction of propagation may be caused by different mechanisms of daytime and nighttime MSTID generation (Kelley & Miller, 1997; Miller et al., 1997).

In the southern hemisphere, particularly in South America, the observations were made mainly during the nighttime MSTIDs (Candido et al., 2008; Duly et al., 2013; Garcia et al., 2000; Paulino et al., 2016; Pimenta et al., 2008; Valladares & Sheehan, 2016). The majority of authors observed that nighttime MSTIDs propagate to northwest. Although, some authors observed nighttime MSTIDs propagating northward and northeastward in the low-latitude region of Brazil (Paulino et al., 2016). On the other hand, there are not many observations of daytime MSTIDs; MacDougall et al. (2011) observed MSTIDs in the northeast of Brazil using

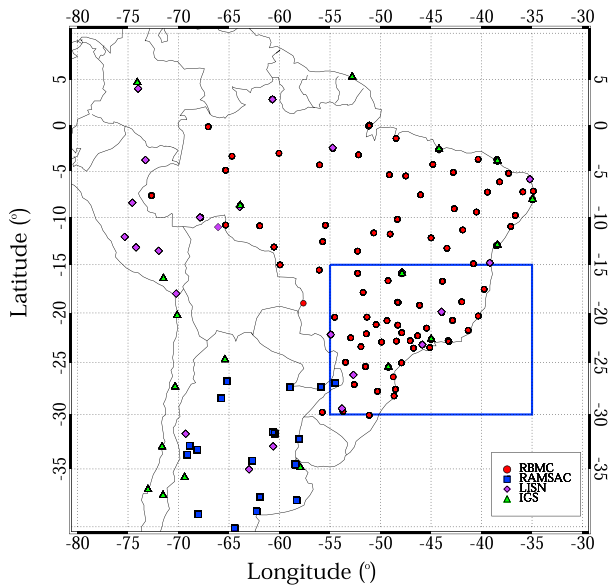


Figure 1. Distribution of ground Global Navigation Satellite Systems (GNSS) receivers, referring to 2014, in South America, maintained by the Rede Brasileira de Monitoramento contínuo dos sistemas GNSS, RAMSAC, and Low latitude Ionospheric Sensor Network networks; some receivers belong to the International GNSS Service network. The blue rectangle is the area used in the present work.

GNSS receivers located in South America, and the GNSS receivers used in the present work are highlighted by the blue rectangle. Each GNSS receiver provides phase and P-code pseudo range at the frequencies of the L band in every 30 s.

The TEC can be calculated using phase delay of each wave frequency L_1 and L_2 along the GNSS satellite and ground receiver, which can be derived using equation (1) (Mannucci et al., 1998).

$$TEC = \frac{1}{40.3} \frac{f_1^2 f_2^2}{f_1^2 - f_2^2} [(L_1 - L_2) - (\lambda_1 N_1 - \lambda_2 N_2) + b_r + b_s], \quad (1)$$

in which L_1 and L_2 are the phase delay of the signal, converted to distance unit; $\lambda_1 N_1$ and $\lambda_2 N_2$ are the integer phase ambiguity; and b_r and b_s are instrumental bias of the satellite and receiver, respectively. The equation (1) cancels the geometric part of the measurement, leaving the frequency-dependent effects such as instrumental delays, wind-up, ionospheric refraction, measurement noise, and multipath. More details can be found in Hofmann-Wellenhof et al. (2012). The goal of this study is to obtain the fluctuation of the TEC to study MSTIDs, following the same procedure of Otsuka et al. (2011, 2013), Kotake et al. (2007), and Tsugawa et al. (2007).

The perturbation component of the TEC (dTEC) is calculated by subtracting a 1 hr running average (centered at ± 30 min) from the original TEC time series (Figueiredo, Wrasse, et al., 2017; Tsugawa et al., 2007). The relative accuracy of the TEC fluctuation is theoretically 0.01–0.02 TEC unit (TECU) (where 1 TECU = 10^{16} el m^{-2}), which corresponds to 1% of the wavelength of the Global Positioning System signal L_1 and L_2 (Spilker & Parkinson, 1996). Then, the perturbation component of the TEC was converted from slant to vertical dTEC using a single-layer model. Furthermore, the TEC data with elevation angles less than 30° were removed in order to reduce the problem of cycle slips.

Two-dimensional maps of the TEC perturbations were made within the area 35° – 55° W and 15° – 30° S, with a time resolution of 30 s and spatial resolution of $0.2^\circ \times 0.2^\circ$ in longitude and latitude. In order to minimize the lack of data in TEC perturbations maps, the grid was smoothed by $1^\circ \times 1^\circ$ in latitude and longitude, same methodology adopted by Figueiredo, Wrasse, et al. (2017). Figure 2 shows an example of a dTEC map on

ionosondes, and they found that daytime MSTIDs have two main propagation directions: south-southeast throughout the year and north from April to September. Jonah et al. (2016) observed four events of daytime MSTIDs, during the summer in south-southeast of Brazil, propagating northeastward. These studies showed us that in the Brazilian sector the direction of propagation of daytime MSTIDs changes according to latitude and seasons. Thus, in order to investigate the characteristics of daytime MSTIDs, its seasonal variability, direction of propagation, and wave generating mechanisms, further study based on a large amount of data extending from low to middle-latitude regions would be necessary.

The present work shows, for the first time, the statistical results of daytime MSTID characteristics using total electron content perturbation (dTEC) maps, obtained in south-southeast of Brazil. In addition, a new methodology was developed to calculate the parameters of MSTIDs observed in dTEC keograms. Lastly, this study attempts to explain the propagation directions of daytime MSTIDs associated with the location of the sources.

2. Data and Method of Analysis

More than 150 GNSS receivers have been installed in Brazil; those are operated by Rede Brasileira de Monitoramento contínuo dos sistemas GNSS and Low latitude Ionospheric Sensor Network; some receivers belong to the International GNSS Service network. Figure 1 shows the

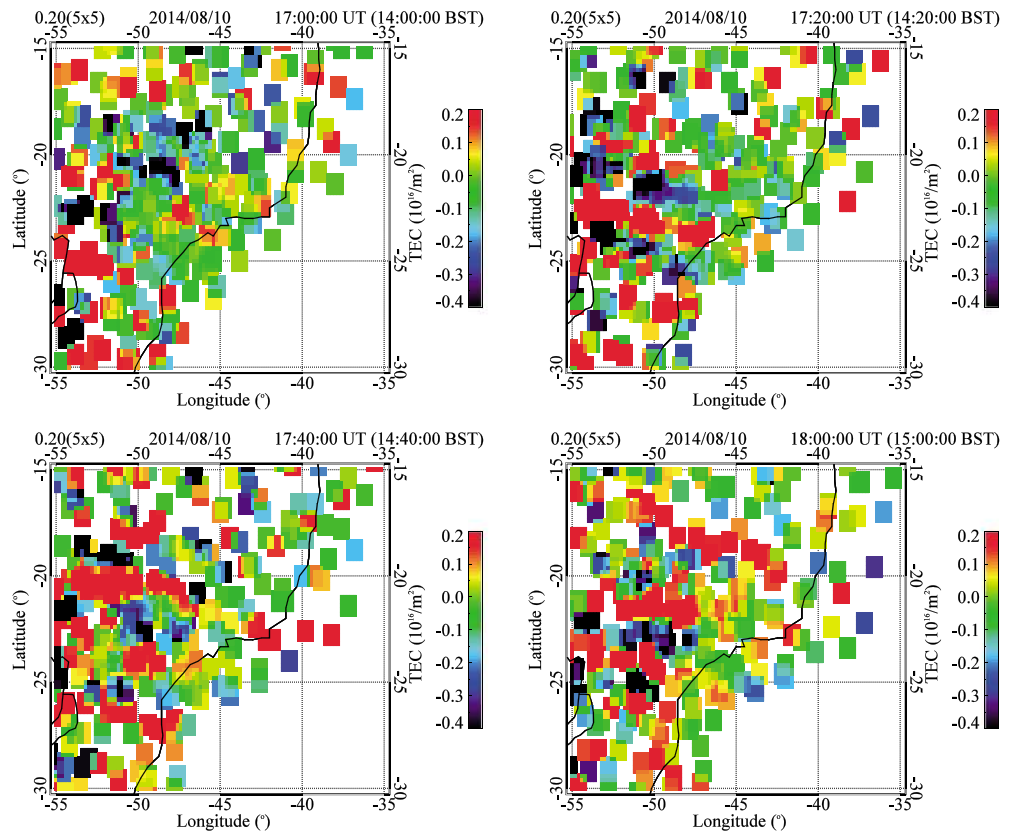


Figure 2. dTEC maps observed in south-southeast of Brazil on 10 August 2014, between 17:00 and 18:00 UT. The images show a medium-scale traveling ionospheric disturbance propagating northeastward.

10 August 2014, between 17:00 and 18:00 UT. One can clearly see a MSTID propagating northeastward over south-southeast of Brazil. An animation of Figure 2 is available through the supporting information related to this paper (see Movie S1). The color codes are in accordance with the disturbance signal, from red (positive) to black (negative).

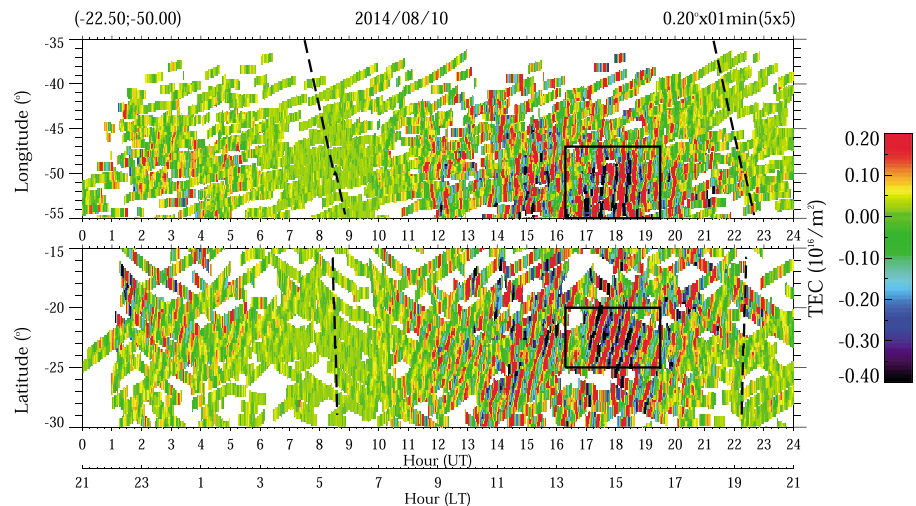


Figure 3. dTEC map keograms of 10 August 2014, for the (top) zonal and (bottom) meridional cut. The black boxes are the region selected for medium-scale traveling ionospheric disturbance analysis. The black dashed lines indicate the solar terminator.

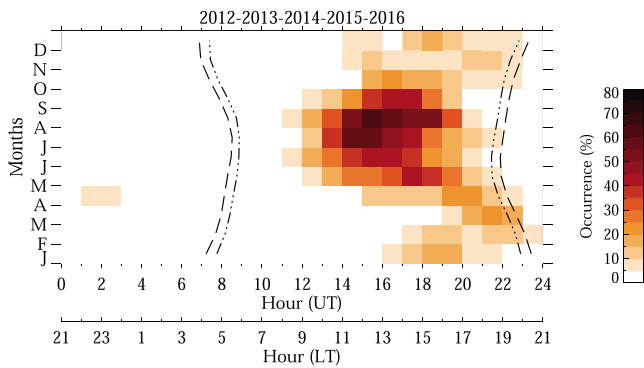


Figure 4. Seasonal variation of medium-scale traveling ionospheric disturbance occurrence rate with the function of local time in south-southeast of Brazil. Data from December 2012 to February 2016 are averaged. The black dashed and dash-dotted lines represent the solar terminator at 300 and 100 km altitude, respectively.

We have investigated time sequences of dTEC maps with a time resolution of 30 s to identify the TEC perturbations by MSTIDs. In order to observe temporal evolution of the perturbation, we used the keogram method. Keogram is made by taking latitudinal and longitudinal cut section of each processed dTEC map image, and, then, taking them to make a time series (time resolution of 1 min), so that the evolution of latitudinal and longitudinal components could be seen on it (e.g., Figueiredo, Wrasse, et al., 2017; Narayanan et al., 2014; Saito et al., 2007; Sobral et al., 2001; Taylor et al., 2009). Figure 3 shows an example of dTEC keogram on 10 August 2014, from 0 to 24 UT. A MSTID can be identified with positive (red) and negative (blue) dTEC lines, highlighted by black boxes in Figure 3. The inclination of the MSTID in the two components indicates the direction of propagation; that is, the inclination of MSTID in the Figure 3 (bottom) starts at ~25°S (17:00 UT) and ends at ~20°S (17:30 UT); this indicates that the MSTID is propagating equatorward. On the other hand, the inclination of MSTID in Figure 3 (top) is almost vertical; starting at ~55°W (17:00 UT) and ends at ~47°W (17:15 UT). It

indicates that the MSTID is propagating eastward. Therefore, the propagation direction is to north-northeast. Moreover, the keogram can show how far it propagated.

A total of 9,488 keograms were made to characterize the observed MSTIDs. First, the MSTIDs are identified by visual inspection, and to validate the MSTIDs, we used the criteria established by Kotake et al. (2007) and Otsuka et al. (2011, 2013); that is, (1) the amplitude of oscillation of dTEC is exceeding 0.2 TECU, (2) the horizontal wavelength is shorter than 1,500 km, (3) the period is less than 60 min, and (4) the oscillation has more than two wavefronts and propagates on the maps or keograms; we assume that the propagation direction is perpendicular to the wavefront of MSTIDs. In addition, we have selected wavefront greater than 3° in latitude and longitude in the keograms.

Figure 3 shows keograms of longitudinal cut at 22.5°S (top) and latitudinal cut at 50°W (bottom) on 10 August 2014. The highlighted areas (by boxes) indicate the MSTID shown in Figure 2. The black dashed lines are the solar terminator in 300 km of altitude. The abscissa determines the universal time and the ordinate distance.

To extract the parameters of MSTIDs, we used the discrete Fourier transform in order to get periodicities in both keograms. The detail of computing procedure is presented in Appendix A. The wave results extracted from the black boxes in the keogram (Figure 3) were wavelength (λ_H) of 370.6 ± 31.3 km, period (τ) of 24.8 ± 1.2 min, horizontal phase velocity (C_H) of 249.0 ± 24.5 m/s, and propagation direction (ϕ) of $9.4 \pm 0.7^\circ$.

3. Results

We have analyzed dTEC data obtained in south-southeastern region of Brazil, including a part of Argentina and Paraguay, from December 2012 to February 2016, and we found 826 MSTIDs, mainly in daytime. The one-year interval was divided into four seasons: summer (December–February), autumn (March–May), winter (June–August), and spring (September–November).

3.1. Seasonal and Local Time Variations

Figure 4 shows seasonal variation of the MSTID monthly occurrence rate as a function of the local time (LT). The occurrence rate is defined as a fraction of the numbers of days of MSTIDs observed against the total number of days of a given month, the same method used by Otsuka et al. (2013).

In Figure 4, we can notice that MSTIDs are strongly dependent on the season and local time. The occurrence rate is high during the period between 10:00 and 17:00 LT, and, especially in the winter months, it

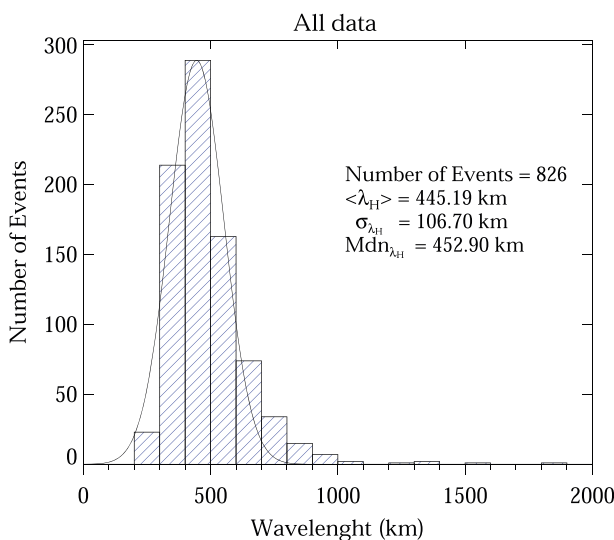


Figure 5. Distribution of the horizontal wavelength of medium-scale traveling ionospheric disturbances observed between December 2012 and February 2016. The solid black line is a Gaussian fit.

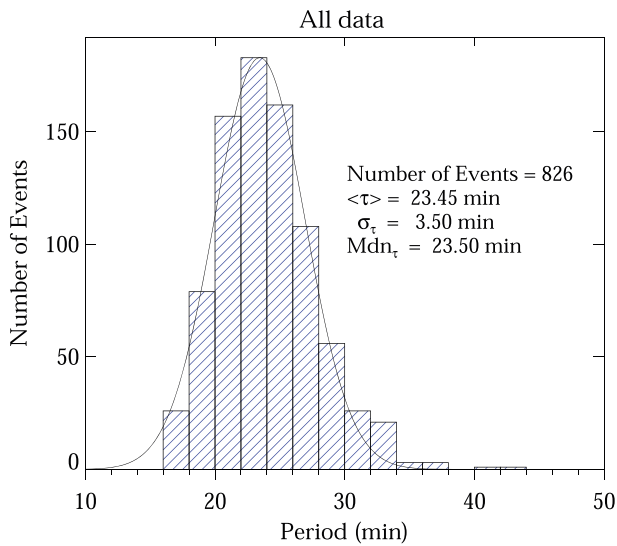


Figure 6. Distribution of the observed period of medium-scale traveling ionospheric disturbances. The solid black line is a Gaussian fit in the data.

3.3. Propagation Direction

Figure 8 shows propagation direction and phase velocity of MSTIDs. As can be seen, the propagation directions are variables. In summer (Figure 8a), the propagation directions are spread out, although the preferential propagation is to southeast. In the autumn (Figure 8b), the MSTIDs propagate mostly toward the north-northeast and there are two clusters of propagation directions: southwest and southeast. On the other hand, in winter (Figure 8c), the propagation directions are only north-northeast, and, in the spring (Figure 8d), there are preferential propagation direction toward north and southeast.

Figure 9 shows occurrence of the propagation directions of MSTID as a function of the time. During the winter (Figure 9c), there is no change in the propagation direction over time. However, in equinoxes (Figures 9b and 9d) and summer solstice (Figure 9a), the propagation directions varied with the LT. These variations occurred

exceeds 60%. During the equinox and the summer solstice, the MSTID occurrence rate is lower than in the winter months, below 30%. In addition, the time of occurrence of MSTIDs in the equinoxes and summer solstice is near to the dusk terminator side.

3.2. Wave Parameters

Figure 5 shows a histogram of the observed horizontal wavelength of MSTIDs. Most of the waves have horizontal wavelength between 300 and 600 km. The distribution is slightly asymmetric. Therefore, we calculated the median, Mdn_{λ_H} (452.90 km), and the standard deviation, σ_{λ_H} (106.70 km). No wave with the wavelength shorter than 200 km was identified.

Figure 6 shows the observed oscillation period of the MSTIDs. It ranged between 15 and 35 min, and few events were found above this range. The median value was 23.50 min with a standard deviation of 3.50 min.

Figure 7 presents the horizontal phase velocity of the MSTIDs. In the figure, it is observed that most of the MSTIDs have a phase velocity with range from 200 to 500 m/s, and a median value of 323.49 m/s with a standard deviation of 80.95 m/s.

late in the afternoon during equinoxes: in the autumn, MSTIDs propagate toward southeast-south-southwest near the dusk; in the spring, MSTIDs propagate to southeast-south, but the time of occurrence is wider, from 12:00 to 19:00 LT.

In the summer (Figure 9a), the highest occurrence of MSTIDs is close to the dusk terminator. The propagation direction is wide as seen in Figure 8a; if we assume that upward gravity waves from the troposphere reach to the thermosphere and generate MSTIDs, the source of the MSTIDs could be in the opposite side of the direction of propagation? This is what we will discuss in the next section.

4. Discussion

From the dTEC map and its keogram, we could study daytime MSTIDs within an area of 35°–55°W and 15°–30°S. The wave characteristics, that is, horizontal wavelength, period, phase velocity, propagation direction, and the seasonal variations, are studied. In the following sections, we compare our results with previous works and discuss the mechanism of generating daytime MSTIDs.

4.1. Seasonal Characteristics

Kotake et al. (2007), Ding et al. (2011), and Otsuka et al. (2011, 2013) have reported that in the NH middle latitudes, the highest occurrence of

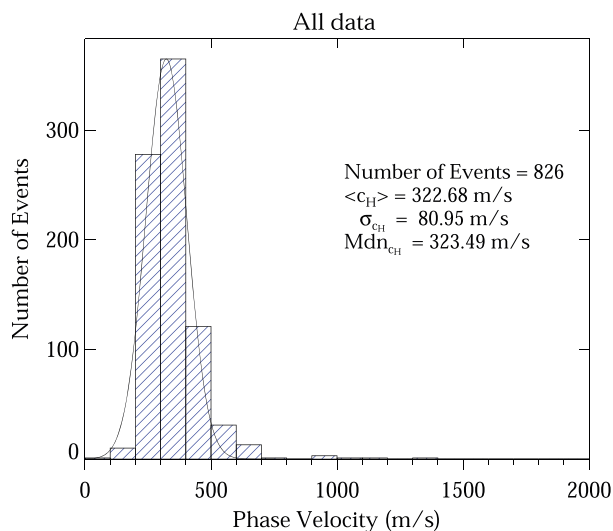


Figure 7. Distribution of the horizontal phase velocity of the observed medium-scale traveling ionospheric disturbances. The solid black line is a Gaussian fit.

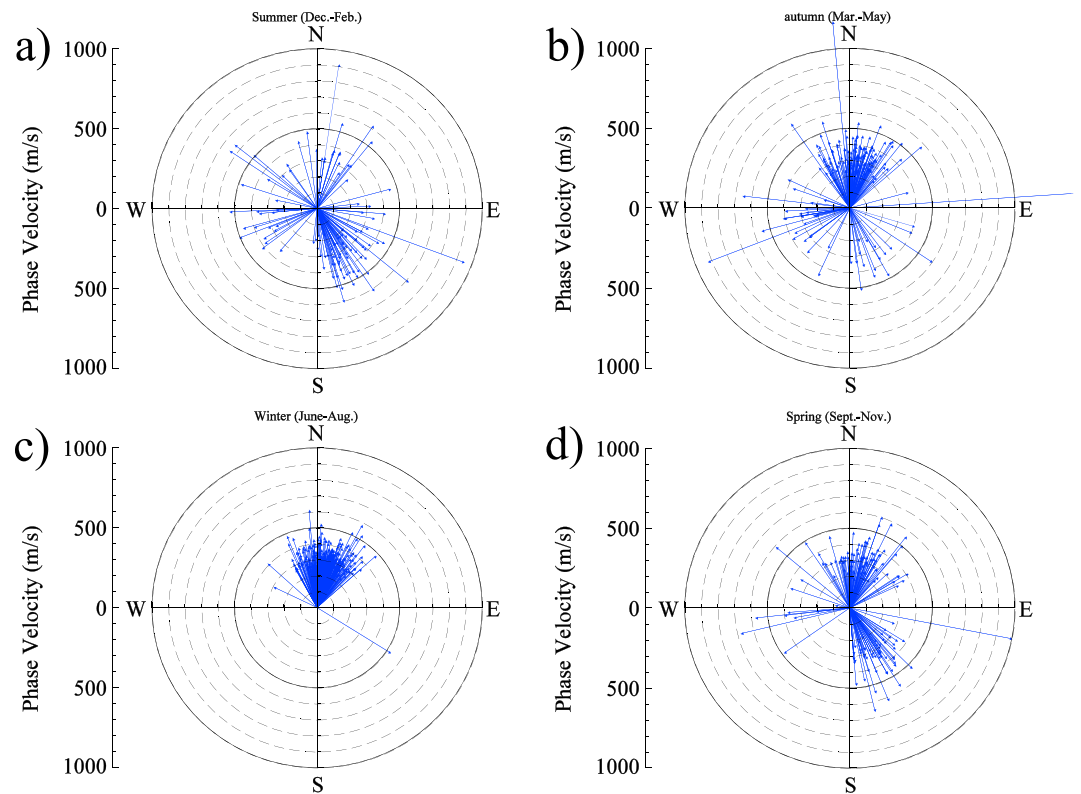


Figure 8. Propagation direction diagrams of medium-scale traveling ionospheric disturbances for (a) summer, (b) autumn, (c) winter, and (d) spring. The circular lines indicate the same phase velocity.

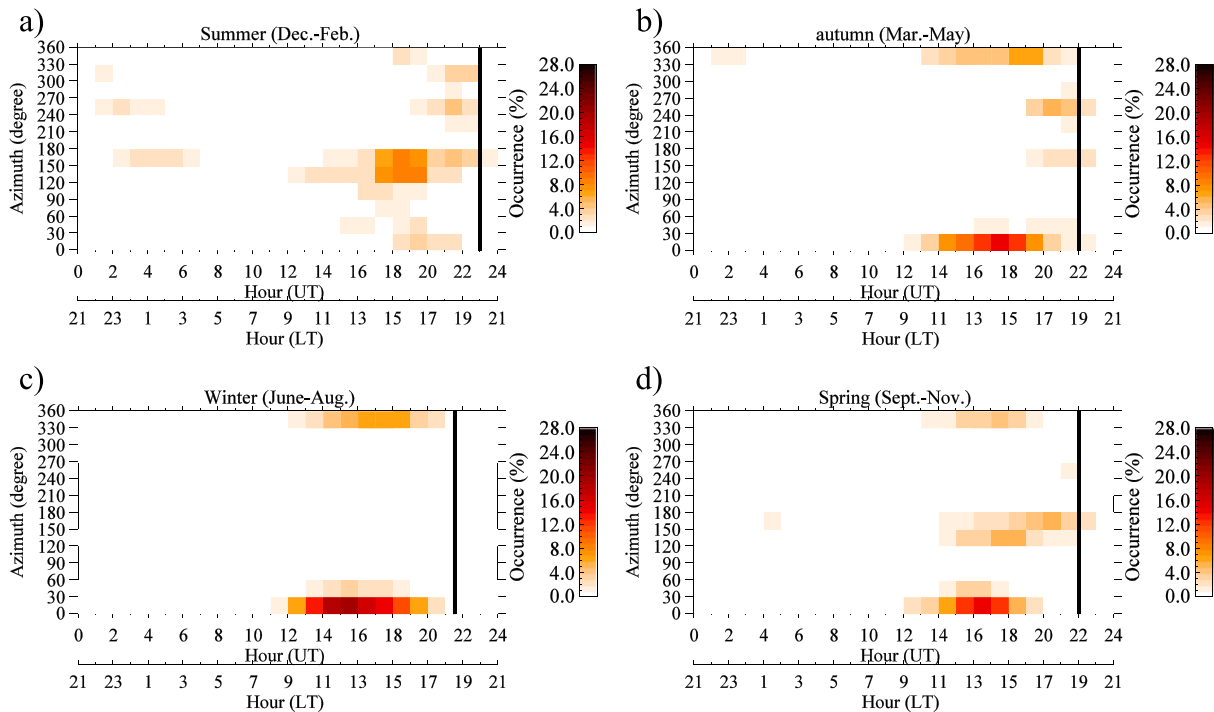


Figure 9. Local time dependency of propagation direction of medium-scale traveling ionospheric disturbances for (a) summer, (b) autumn, (c) winter, and (d) spring. The black continues lines are the dusk terminator.

daytime MSTIDs was during the winter (between November and February). Park et al. (2015) observed MSTIDs in a region between 300 and 400 km altitude, using the density measurements of the Challenging Minisatellite Payload (CHAMP) satellite. They observed the highest occurrence of MSTIDs over South America during the winter (June). Also, Forbes et al. (2016) and Liu et al. (2017) observed MSTIDs with the horizontal wavelength of 100 to 700 km, in the region between 200 and 260 km altitude, from the measurements of perturbations in the neutral density, measured by Gravity Field and Steady-State Ocean Circulation Explorer (GOCE) satellite. The authors observed that the highest occurrence of MSTIDs in South America was in the winter months. Our present observations showed comparable results with the previous observations. The low occurrences during the equinoxes and summer are also similar to the results of Park et al. (2015), Forbes et al. (2016), and Liu et al. (2017).

Kotake et al. (2007) and Otsuka et al. (2011, 2013) observed that the occurrence of MSTIDs during the winter was before 12:00 LT, which is different from our present results. Ávila et al. (2015) investigated the occurrence of lightning by Lightning Imaging Sensor onboard the Tropical Rainfall Measuring Mission satellite (<http://thunder.msfc.nasa.gov>), and they associated it with the occurrence of convective storm. The authors observed, during the equinox and summer months, that the time of convective storm occurrence in the Southern region of Brazil and Northeastern Argentina was between 14:00 and 18:00 LT. On the other hand, during the winter, Ávila et al. (2015) observed that most convective storms in southern Brazil and northeastern Argentina occurred between 0:00 and 8:00 LT. The MSTIDs, in the present work, were observed most frequently during daytime between 11 and 15 LT in winter and near to dusk solar terminator (17–19 LT) in the other seasons. Therefore, the convective storms show a good correlation with the MSTIDs observed during the equinox and summer. However, during the winter months, it is not possible to verify a correlation between MSTID observation and the occurrence of lightening.

Abdu et al. (2015) analyzed the digisonde data from October to November 2001, at three sites in the equatorial region of Brazil, during the period of plasma bubbles. They found that the *F*-layer oscillations between 12:00 LT and dusk period may be the precursor of plasma bubbles.

The differences in the time of occurrence, seen in Figure 9 and observed in other works, such as Kotake et al. (2007) and Otsuka et al. (2011, 2013), could be due to different mechanisms of MSTID generation and local atmosphere characteristics, for example, density, wind, temperature, thermal diffusivity, and upward gravity waves associated with convective storms.

A pertinent question is why MSTIDs did occur more in the winter than in the summer. Miyoshi et al. (2014) studied seasonal variations of upward gravity wave propagations during the summer and winter solstices using the general circulation model. The authors observed that in South America, the energy (potential plus kinetics) is similar at 120 km altitude in winter and summer, with winter being slightly higher (Miyoshi et al., 2014, Figures 12b and 7b). In the thermosphere at 300 km, on the other hand, the energy of the gravity waves is significantly high in the winter (Miyoshi et al., 2014, Figure 6b), while in summer the gravity waves have no condition to propagate vertically (Miyoshi et al., 2014, Figure 12a). Miyoshi et al. (2009) concluded that high-frequency gravity waves generated in the troposphere propagate to the thermosphere inducing wave structures in the zonal wind in the upper atmosphere. Thus, Miyoshi et al. (2014) suggested that the mechanism that blocks the vertical propagation of the gravity waves is the filtering effect of zonal Wind between 100 and 200 km altitude in 20°S. During the winter, the zonal background wind, between 100 and 200 km of altitude, is westward (Miyoshi et al., 2014, Figure 4a), so gravity waves propagate easily eastward and have a higher vertical wavelength due to the Doppler shift. In the summer the background wind between 100 and 200 km flows westward and eastward (Y. Miyoshi, private communication, 2016), so the upward gravity waves that move eastward or westward will decrease the vertical wavelength due to Doppler shift. Therefore, the gravity wave may not have enough energy to propagate vertically and disturb the *F* layer. Further investigations and simulations are needed to validate this hypothesis.

In the present observation we could not notice nighttime MSTIDs, with the exception of some occasional cases. Some nighttime MSTID observation has been reported by Paulino et al. (2016). They observed it using OI 630.0 nm airglow images over Brazilian northeast and found horizontal wavelengths (λ_{\perp}) ranged from 100 to 200 km, period (τ) between 10 and 35 min, and phase velocity (C_{\perp}) from 30 to 180 m/s. Owing to our limitation of observation technique (horizontal wavelength less than 200 km is not possible to depict on the dTEC map), we could not see such relatively short wavelength MSTIDs.

4.2. Wave Parameters

Kotake et al. (2007) obtained a horizontal wavelength between 100 and 450 km, while Otsuka et al. (2011) observed horizontal wavelengths of 100 to 600 km during all the seasons. On the other hand, the present study observed a further wide range of horizontal wavelength, as shown in Figure 5. The periods observed in the present work have the same order of magnitude of previous works, for example, Kotake et al. (2007) and Otsuka et al. (2011). It is worth noting that they used the same a 1 hr running average subtraction. Kotake et al. (2007) and Otsuka et al. (2011) obtained horizontal phase velocities of 80 to 180 m/s, which are below the values of the present study. On the other hand, MacDougall et al. (2011) observed MSTIDs in the northeast of Brazil using ionosondes. They observed horizontal phase velocities between 150 and 300 m/s, which have the same order of the present study.

According to Vadas (2007), gravity waves in the thermosphere with the horizontal phase velocity between 300 and 600 m/s and horizontal wavelength longer than ~ 500 km are less susceptible to dissipation, damping and kinetic viscosities, and thermal diffusivity, see also Vadas and Fritts (2005). Furthermore, high-frequency gravity waves (≤ 60 min) can propagate from low atmosphere and dissipate at altitudes above 200 km (Vadas, 2007). Most of the wave parameters in the present work are within the range presented in the Vadas (2007) model. Therefore, it may be that MSTIDs can originate in the troposphere.

4.3. Propagation Direction

Kotake et al. (2007) and Otsuka et al. (2011) observed daytime MSTIDs that propagated equatorward during the winter and southeastward during the summer. The current results are similar to those observed in the NH, at least for the winter period. However, for the other seasons, our present results are different.

MacDougall et al. (2011) found that propagation directions of MSTIDs observed after sunset in Brazilian Northeast are not compatible with propagation directions of MSTIDs observed at midlatitudes, which propagate approximately westward after sunset (e.g., Kotake et al., 2007; Otsuka et al., 2011). The current study corroborates the observations of MacDougall et al. (2011).

Around 74% of MSTIDs propagate to northwest, north, and northeast. To explain this behavior, we consider three hypotheses. The first one is based on the study presented by Hooke (1968); he formulated a linear theory that uses a description of the relationship between plasma density perturbations and neutral wind oscillation caused by gravity waves. According to his theory, the gravity waves propagating equatorward would have greater amplitude of disturbances in the TEC than those propagating in other directions. This behavior might be related to the fact that gravity waves are oscillations of neutral constituents. Through neutral-ion collisions, the ions in the *F* region move along the geomagnetic field lines and the motion of those ions is restricted to this direction because the ion gyrofrequency is much higher than ion-neutral collision frequency (Hooke, 1970). However, in the South American continent, the magnetic equator has a very pronounced declination (between 15 and 20°W in south-southeast of Brazil, declination calculated for 2015). If we assume the first hypothesis as the main mechanism to explain the direction of propagation, diurnal MSTIDs should propagate only toward the magnetic field lines. Most daytime MSTIDs show direction of propagation to the north-northeast ($\sim 55\%$), suggesting that another mechanism should be responsible for the direction of propagation of daytime MSTIDs.

The second hypothesis may be associated with gravity waves filtering by atmospheric neutral wind (e.g., Medeiros et al., 2003, and references therein). The gravity waves filtering by atmospheric neutral wind process occur when the wind speed is equal to the MSTID velocity. When this occurs, it is called the critical level and, as a result, the gravity waves cannot propagate upward (Vadas, 2007). Barros et al. (2018), Figueiredo, Buriti, et al. (2017), and Makela et al. (2013) reported that the nighttime thermospheric neutral wind magnitude, observed by Fabry-Perot interferometer in the Brazilian northeast, is not greater than 150 m/s. Moreover, Drob et al. (2015) updated the Horizontal Wind Model and verified that the diurnal thermospheric neutral wind does not exceed 160 m/s on quiet days. Therefore, the gravity waves filtering by atmospheric neutral wind hypothesis as the main mechanism to explain the propagation direction of daytime MSTIDs is unlikely, because daytime MSTIDs have horizontal phase velocities (see Figure 7), much greater than the magnitude of the wind in the thermosphere.

The third hypothesis talks about the location of the possible sources of MSTIDs as a mechanism that can determine the propagation direction of MSTIDs. MacDougall et al. (2011) found that daytime MSTIDs have

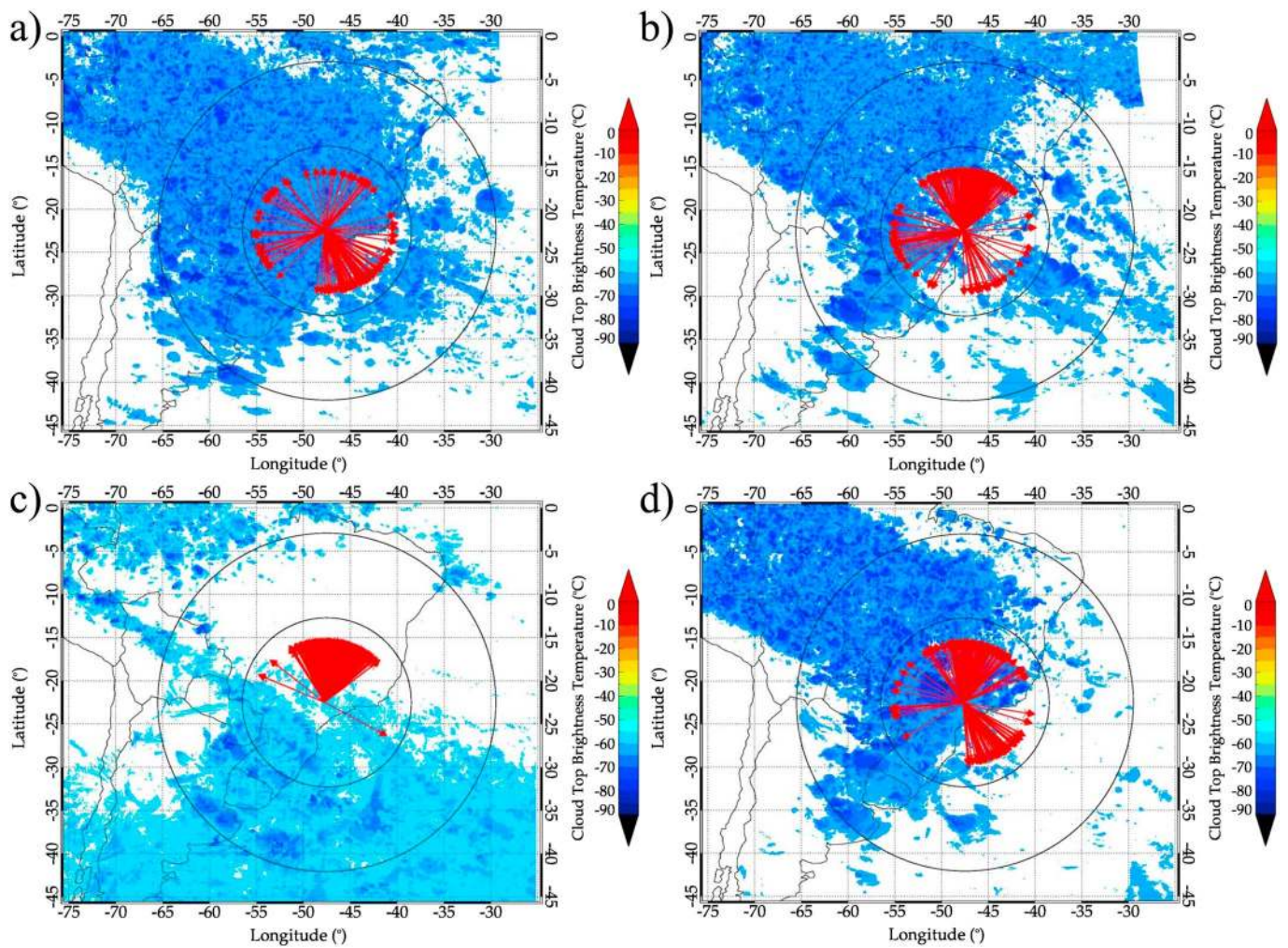


Figure 10. Cloud top brightness temperature maps with temperatures below -55°C overplotted between December 2012 and February 2016. The red arrows indicate the propagation direction of medium-scale traveling ionospheric disturbances observed in each season: (a) summer, (b) autumn, (c) winter, and (d) spring. Two time zones were selected to plot the maps: $12:00 \pm 1:00$ UT, for winter, and $16:00 \pm 1:00$ UT, for the other seasons. The black circles correspond to 1,000 and 2,000 km radius on the maps.

two main propagation directions: south-southeast, throughout the year, and north, only from April to September. The authors suggest that the MSTIDs that propagate to south-southeast are derived from upward gravity waves from the Intertropical Convergence Zone. On the other hand, the authors did not attribute a source to MSTIDs propagating northward. The propagation direction observed during the winter period in the present study pointed only to the north-northeast directions. Although their observations were located near the equator and our present observation were around low to middle latitudes, the similarity on the propagation direction during the winter called our attention.

4.3.1. SOURCE OF MSTIDs

As seen in Figure 9, propagation directions change according to the seasons and LT. If we assume that daytime MSTIDs are caused by upward gravity waves, one of the possible mechanisms may be associated with strong convective activity that occurs around the observation region. In this way, we compared the observed propagation directions of MSTIDs with the location of convective clouds in the troposphere.

The parameter used to measure the intensity of the convection cloud is the cloud top brightness temperature (CTBT). Temperatures between 208 K (-65°C) and 253 K (-20°C) can be used to define areas associated with Cumulonimbus or deep convective clouds (Inoue et al., 2008). In this study we used CTBT maps with two

upper limit temperatures: -55 and -45 °C. The maps with CTBT below -55 °C are used to highlight the deep convection throughout the years, that is, between December 2012 and February 2016. On the other hand, CTBT maps with temperatures lower than -45 °C are considered as a convection region and possible MSTID sources. The infrared thermal images are obtained by the Geostationary Operational Environmental Satellite System 13 (GOES 13) with a spatial resolution of 4×4 km, and available in binary files by the scientific cooperation between GOES 13 and Center for Weather Forecasting and Climate Studies in Brazil. According to Vadas (2007), gravity waves with wavelengths shorter than 500 km take around 1 to 3 hr to propagate from the troposphere to the thermosphere. Based on the results of the Vadas (2007) model, we selected two time zones referring to the time of occurrence of MSTIDs observed in the seasons: $12:00 \pm 1:00$ UT for winter and $16:00 \pm 1:00$ UT for the other seasons. Figure 10 shows CTBT maps over South America. Each map corresponds to a different season, overplots all of the maps taken at 12:00 UT (winter) and 16:00 UT (spring, summer, and autumn) from December 2012 to February 2016. The black circles, with 1,000 and 2,000 km radius, were plotted in the figure as distance reference. The red vectors represent the direction of propagation of MSTIDs. It is clearly seen in the winter panel (Figure 10c) that the cloud convection activities were localized only at the south and southeast of the observer (~ 23 S). The specific propagation direction of MSTIDs during the winter is quite significant. According to Vadas (2007), gravity waves with $\lambda_H \leq 500$ km, $C_H \geq 100$ m/s, and $\tau \leq 60$ min propagate horizontally up to $\sim 2,000$ km from the troposphere until they dissipate at altitudes between 150 and 250 km. The circle of 2,000 km therefore may indicate a possible limit of distance for propagation of MSTIDs.

In Figure 10c, it is observed that the MSTID propagation directions are to north and northeast during the winter. MacDougall et al. (2011) and Paulino et al. (2016) also reported MSTIDs propagating north-northeastward during the winter, in equatorial latitudes of Brazil. It might suggest that the source of MSTIDs in equatorial and middle latitudes of Brazil is the same. The deep convection activities in the south of Brazil during the winter are highly related to the jet stream associated with cold fronts (Zhang, 2004).

In the other seasons (Figures 10a, 10b, and 10d), deep convections associated with cumulus nimbus clouds can be observed throughout Brazil. The direction of propagation of MSTIDs in these seasons is virtually for all directions, which suggests that the deep convections might be the sources of the MSTIDs. In order to further investigate, however, it is necessary to have a better idea whether the observed MSTIDs were originated from the troposphere or from any other wave sources. The ray tracing method (e.g., Vadas, 2007; Vadas & Crowley, 2010) would be helpful to understand.

5. Conclusion

In this paper, about three years of ground-based GNSS receiver data were used to make dTEC maps and keograms with the goal of observing the characteristics of MSTIDs in the south-southeast of Brazil. The main results and conclusions obtained in this work were the following:

1. A total of 826 daytime MSTIDs were observed, presenting the following characteristics: horizontal wavelength, period, and horizontal phase velocity median of 452 ± 107 km, 24 ± 5 min, and 323 ± 81 m/s, respectively.
2. MSTIDs were observed in all months. The highest occurrence was in the winter months (44%), followed by the equinoxes (42%), and summer solstice (14%). The time of occurrence was in the early afternoon, in the winter solstices, and during the solar terminator passage, in the summer solstice. Moreover, we could not observe nighttime MSTIDs, with the exception of some occasional cases.
3. The propagation direction of MSTID was not isotropic. It was highly anisotropic during the winter, propagating to north-northeastward. On the other hand, in the other seasons, daytime MSTIDs propagated in all directions, with some clusters.
4. When the observed MSTID parameters are compared with the numerical model results, we can suggest that the possible source of daytime MSTIDs might be deep convection storms in the troposphere. In winter, the convection region associated with jet stream and cold fronts is found in the Brazilian South. In summer and equinoxes, the deep convection region is associated with cumulus nimbus clouds, located all over Brazil, but during the summer and equinox, the correlation between direction of propagation of MSTIDs and CTBT maps is low. Therefore, further studies using ray tracing would be necessary to investigate the sources of MSTIDs.

As a perspective for future works, we present some questions: the investigation of daytime MSTIDs near the geomagnetic equatorial region, which may provide us better understanding whether daytime MSTIDs could act as a precursor of plasma bubble generation, furthermore the study of MSTIDs in the American sector, associated with slow magnetosonic waves before the dusk solar terminator at conjugated points, as studied by Afraimovich et al. (2009). Other question that needs some theoretical input is why MSTIDs at low latitudes are not generated by dawn terminator.

Appendix A

In order to extract the parameters of MSTIDs, we have developed a method of spectral analysis, using discrete Fourier transform.

First, it is necessary to select a region containing the oscillation in the keogram components, as shown in Figure 3. It is important to notice that the area to be analyzed must be the same in each of the components. Then, we apply it to discrete Fourier transform (equation (A1)) in the selected set of time series.

$$F(\omega) = \sum_{n=0}^{N-1} f(t) e^{-\frac{2\pi n i}{N}}, \quad (A1)$$

in which $F(\omega)$ is the transform of the Fourier function $f(t)$, $\omega = 0, \dots, N - 1$ is the frequency index, and N is the number of points in time series in selected regions.

Then, the cross spectrum is calculated, defined by equation (A2):

$$C(\omega) = F_S(\omega) F_{S+1}^*(\omega), \quad (A2)$$

in which $C(\omega)$ is the cross spectrum between two time series and $F_S(\omega)$ and $F_{S+1}^*(\omega)$ represent the Fourier transform of the series $f_S(t)$ and $f_{S+1}(t)$, respectively. $F_{S+1}^*(\omega)$ is the complex conjugate of $F_{S+1}(\omega)$. The one-dimensional cross power spectrum is defined by the quadratic modulus, $|C^2|$. If the number of time series selected is S , the resulting cross power spectrum will be the average of $S - 1$ cross power spectrum computed.

The amplitude of the cross power spectrum is expressed by $2\sqrt{|C^2|}$, with the phase of the cross spectrum being defined by

$$\Delta\psi = \text{tg}^{-1} \left\{ \frac{\text{Im}(C(\omega))}{\text{Re}(C(\omega))} \right\}, \quad -\pi \leq \psi \leq \pi.$$

For the frequency ω , in which the amplitude is maximum, the phase of the cross spectrum is the phase difference caused by the wave propagation between these time series.

The equations used to determine the parameters are as follows:

1. Period (min.):

$$\tau = \frac{1}{|f(\omega)|};$$

2. The wavelength (km) for the zonal and meridional components ($\lambda_{NS, EW}$):

$$\lambda_{NS,EW} = \frac{\Delta d}{\Delta\psi / 360^\circ},$$

in which Δd represents the distance between the time series.

3. Horizontal wavelength (km):

$$\lambda_H = \frac{\lambda_{NS} \lambda_{EW}}{\sqrt{\lambda_{NS}^2 + \lambda_{EW}^2}};$$

4. Finally, the horizontal phase velocity, C_H (m/s), and phase of propagation direction, ϕ ($^\circ$), can be obtained by

$$C_H = \frac{\lambda_H}{\tau},$$

$$\phi = \cos^{-1} \left(\frac{\lambda_H}{\lambda_{NS}} \right).$$

To validate the method, an analysis was performed in order to identify the parameters of the MSTIDs. We simulated waves with wavelength between 100 and 600 km, step of 50 km; period between 10 and 120 min, cadence of 10 min; and propagation direction from 0 to 360 $^\circ$, with step of 30 $^\circ$. In total, more than 143 combinations were analyzed and the results showed that the uncertainties are less than 10% in λ , τ , C_H , and ϕ .

Acknowledgments

The GPS data used in this study were provided via FTP servers of RBMC and EMBRACE. The CTBT maps were provided by the Center for Weather Forecasting and Climate Studies (CPTEC/INPE). The present work was supported by the Conselho Nacional de Desenvolvimento Científico e Tecnológico (CNPq), under the processes 150569/2017-3, 161894/2015-1, 310926/2014-9, 305461/2015-0, 141823/2016-0, and 169815/2017-0; Coordenação de Aperfeiçoamento de Pessoal de Nível Superior (CAPES), under the process BEX4488/14-8; and JSPS KAKENHI, under the process JP 15H05815 and JP 16H06286 grant.

References

- Abdu, M. A., Souza, J. R., Kherani, E. A., Batista, I. S., MacDougall, J. W., & Sobral, J. H. A. (2015). Wave structure and polarization electric field development in the bottomside F layer leading to postsunset equatorial spread f . *Journal of Geophysical Research: Space Physics*, *120*, 6930–6940. <https://doi.org/10.1002/2015JA021235>
- Afraimovich, E. L., Edemskiy, I. K., Voeykov, S. V., Yasyukevich, Y. V., & Zhivetiev, I. V. (2009). The first GPS-TEC imaging of the space structure of m_s wave packets excited by the solar terminator. *Annales Geophysicae*, *27*(4), 1521–1525. <https://doi.org/10.5194/angeo-27-1521-2009>
- Amorim, D. C. M., Pimenta, A. A., Bittencourt, J. A., & Fagundes, P. R. (2011). Long term study of medium-scale traveling ionospheric disturbances using 630 nm all sky imaging and ionosonde over Brazilian low latitudes. *Journal of Geophysical Research: Space Physics*, *116*, A06312. <https://doi.org/10.1029/2010JA016090>
- Ávila, E. E., Bürgesser, R. E., Castellano, N. E., & Nicora, M. G. (2015). Diurnal patterns in lightning activity over South America. *Journal of Geophysical Research: Atmospheres*, *120*, 3103–3113. <https://doi.org/10.1002/2014JD022965>
- Barros, D., Takahashi, H., Wrasse, C. M., & Figueiredo, C. A. O. B. (2018). Characteristics of equatorial plasma bubbles observed by TEC map based on ground-based GNSS receivers over South America. *Annales Geophysicae*, *36*(1), 91–100. <https://doi.org/10.5194/angeo-36-91-2018>
- Candido, C. M. N., Pimenta, A. A., Bittencourt, J. A., & Becker-Guedes, F. (2008). Statistical analysis of the occurrence of medium-scale traveling ionospheric disturbances over Brazilian low latitudes using 630.0 nm emission all-sky images. *Geophysical Research Letters*, *35*, L17105. <https://doi.org/10.1029/2008GL035043>
- Ding, F., Wan, W., Xu, G., Yu, T., Yang, G., & Wang, J. S. (2011). Climatology of medium-scale traveling ionospheric disturbances observed by a GPS network in Central China. *Journal of Geophysical Research: Space Physics*, *116*, A09327. <https://doi.org/10.1029/2011JA016545>
- Drob, D. P., Emmert, J. T., Meriwether, J. W., Makela, J. J., Doornbos, E., Conde, M., et al. (2015). An update to the Horizontal Wind Model (HWM): The quiet time thermosphere. *Earth and Space Science*, *2*, 301–319. <https://doi.org/10.1002/2014EA000089>
- Duly, T. M., Chapagain, N. P., & Makela, J. J. (2013). Climatology of nighttime medium-scale traveling ionospheric disturbances (MSTIDs) in the Central Pacific and South American sectors. *Annales Geophysicae*, *31*(12), 2229–2237. <https://doi.org/10.5194/angeo-31-2229-2013>
- Figueiredo, C. A. O. B., Burity, R. A., Paulino, I., Meriwether, J. W., Makela, J. J., Batista, I. S., et al. (2017). Effects of the midnight temperature maximum observed in the thermosphere–ionosphere over the northeast of Brazil. *Annales Geophysicae*, *35*(4), 953–963. <https://doi.org/10.5194/angeo-35-953-2017>
- Figueiredo, C. A. O. B., Wrasse, C. M., Takahashi, H., Otsuka, Y., Shiokawa, K., & Barros, D. (2017). Large-scale traveling ionospheric disturbances observed by GPS dTEC maps over North and South America on Saint Patrick's Day storm in 2015. *Journal of Geophysical Research: Space Physics*, *122*, 4755–4763. <https://doi.org/10.1002/2016JA023417>
- Forbes, J. M., Bruinsma, S. L., Doornbos, E., & Zhang, X. (2016). Gravity wave-induced variability of the middle thermosphere. *Journal of Geophysical Research: Space Physics*, *121*, 6914–6923. <https://doi.org/10.1002/2016JA022923>
- Garcia, F. J., Kelley, M. C., Makela, J. J., & Huang, C. S. (2000). Airglow observations of mesoscale low velocity traveling ionospheric disturbances at midlatitudes. *Journal of Geophysical Research*, *105*, 18,407–18,415. <https://doi.org/10.1029/1999JA000305>
- Garcia, R. F., Bruinsma, S., Massarweh, L., & Doornbos, E. (2016). Medium-scale gravity wave activity in the thermosphere inferred from GOCE data. *Journal of Geophysical Research: Space Physics*, *121*, 8089–8102. <https://doi.org/10.1002/2016JA022797>
- Hernandez-Pajares, M., Juan, J. M., & Sanz, J. (2006). Medium-scale traveling ionospheric disturbances affecting GPS measurements: Spatial and temporal analysis. *Journal of Geophysical Research*, *111*, A07511. <https://doi.org/10.1029/2005JA011474>
- Hernandez-Pajares, M., Juan, J. M., Sanz, J., & Aragón-Ángel, A. (2012). Propagation of medium scale traveling ionospheric disturbances at different latitudes and solar cycle conditions. *Radio Science*, *47*, RS0K05. <https://doi.org/10.1029/2011RS004951>
- Hines, C. O. (1960). Internal atmospheric gravity waves at ionospheric heights. *Canadian Journal of Physics*, *38*(11), 1441–1481. <https://doi.org/10.1139/p60-150>
- Hofmann-Wellenhof, B., Lichtenegger, H., & Collins, J. (2012). *Global positioning system: Theory and practice*. Vienna: Springer. 9783709132975
- Hooke, W. H. (1968). Ionospheric irregularities produced by internal atmospheric gravity waves. *Journal of Atmospheric and Terrestrial Physics*, *30*(5), 795–823. [https://doi.org/10.1016/S0021-9169\(68\)80033-9](https://doi.org/10.1016/S0021-9169(68)80033-9)
- Hooke, W. H. (1970). The ionospheric response to internal gravity waves: 1. The F2 region response. *Journal of Geophysical Research*, *75*(28), 5535–5544. <https://doi.org/10.1029/JA075i028p05535>
- Hunsucker, R. D. (1982). Atmospheric gravity waves generated in the high-latitude ionosphere: A review. *Reviews of Geophysics*, *20*, 293–315.
- Inoue, T., Satoh, M., Miura, H., & Mapes, B. (2008). Characteristics of cloud size of deep convection simulated by a global cloud resolving model over the western tropical Pacific. *Journal of the Meteorological Society of Japan*, *86*, 1–15.
- Jonah, O., Kherani, E., & Paula, E. D. (2016). Observation of TEC perturbation associated with medium-scale traveling ionospheric disturbance and possible seeding mechanism of atmospheric gravity wave at a Brazilian sector. *Journal of Geophysical Research: Space Physics*, *121*, 2531–2546.

- Kelley, M. C. (2011). On the origin of mesoscale TIDs at midlatitudes. *Annales Geophysicae*, 29(2), 361–366. <https://doi.org/10.5194/angeo-29-361-2011>
- Kelley, M. C., & Miller, C. A. (1997). Electrodynamics of midlatitude spread F3. Electrohydrodynamic waves? A new look at the role of electric fields in thermospheric wave dynamics. *Journal of Geophysical Research*, 102, 11,539–11,547. <https://doi.org/10.1029/96JA03841>
- Kotake, N., Otsuka, Y., Ogawa, T., Tsugawa, T., & Saito, A. (2007). Statistical study of medium-scale traveling ionospheric disturbances observed with the GPS networks in southern California. *Earth, Planets and Space*, 59(2), 95–102. <https://doi.org/10.1186/BF03352681>
- Liu, H., Pedatella, N., & Hocke, K. (2017). Medium-scale gravity wave activity in the bottomside F region in tropical regions. *Geophysical Research Letters*, 44, 7099–7105. <https://doi.org/10.1002/2017GL073855>
- MacDougall, J., Abdu, M., Batista, I., Buriti, R., Medeiros, A., Jayachandran, P., & Borba, G. (2011). Spaced transmitter measurements of medium scale traveling ionospheric disturbances near the equator. *Geophysical Research Letters*, 38, L16806. <https://doi.org/10.1029/2011GL048598>
- Makela, J. J., Fisher, D. J., Meriwether, J. W., Buriti, R. A., & Medeiros, A. F. (2013). Near-continual ground-based nighttime observations of thermospheric neutral winds and temperatures over equatorial Brazil from 2009 to 2012. *Journal of Atmospheric and Solar - Terrestrial Physics*, 103, 94–102. <https://doi.org/10.1016/j.jastp.2012.11.019>
- Mannucci, A. J., Wilson, B. D., Yuan, D. N., Ho, C. H., Lindqwister, U. J., & Runge, T. F. (1998). A global mapping technique for GPS-derived ionospheric total electron content measurements. *Radio Science*, 33, 565–582. <https://doi.org/10.1029/97RS02707>
- Medeiros, A., Taylor, M. J., Takahashi, H., Batista, P., & Gobbi, D. (2003). An investigation of gravity wave activity in the low-latitude upper mesosphere: Propagation direction and wind filtering. *Journal of Geophysical Research*, 108(D14), 4411.
- Miller, C. A., Swartz, W. E., Kelley, M. C., Mendillo, M., Nottingham, D., Scall, J., & Reinisch, B. (1997). Electrodynamics of midlatitude spread F: 1. Observations of unstable, gravity wave-induced ionospheric electric fields at tropical latitudes. *Journal of Geophysical Research*, 102, 11,521–11,532. <https://doi.org/10.1029/96JA03839>
- Miyoshi, Y., & Fujiwara, H. (2009). Gravity waves in the equatorial thermosphere and their relation to lower atmospheric variability. *Earth Planets Space*, 61, 471–478.
- Miyoshi, Y., Fujiwara, H., Jin, H., & Shinagawa, H. (2014). A global view of gravity waves in the thermosphere simulated by a general circulation model. *Journal of Geophysical Research: Space Physics*, 119, 5807–5820. <https://doi.org/10.1002/2014JA019848>
- Munro, G. H. (1948). Short-period changes in the F region of the ionosphere. *Nature*, 162(4127), 886–887. <https://doi.org/10.1038/162886a0>
- Narayanan, V. L., Shiokawa, K., Otsuka, Y., & Saito, S. (2014). Airglow observations of nighttime medium-scale traveling ionospheric disturbances from Yonaguni: Statistical characteristics and low-latitude limit. *Journal of Geophysical Research: Space Physics*, 119, 9268–9282. <https://doi.org/10.1002/2014JA020368>
- Otsuka, Y., Kotake, N., Shiokawa, K., Ogawa, T., Tsugawa, T., & Saito, A. (2011). Aeronomy of the Earth's atmosphere and ionosphere. In *Statistical Study of Medium-Scale Traveling Ionospheric Disturbances Observed With a GPS Receiver Network in Japan* (pp. 291–299). Dordrecht, Netherlands: Springer. 978-94-007-0326-1
- Otsuka, Y., Suzuki, K., Nakagawa, S., Nishioka, M., Shiokawa, K., & Tsugawa, T. (2013). GPS observations of medium-scale traveling ionospheric disturbances over Europe. *Annales Geophysicae*, 31(2), 163–172. <https://doi.org/10.5194/angeo-31-163-2013>
- Park, J., Lühr, H., Nishioka, M., & Kwak, Y.-S. (2015). Plasma density undulations correlated with thermospheric neutral mass density in the daytime low-latitude to midlatitude topside ionosphere. *Journal of Geophysical Research: Space Physics*, 120, 6669–6678. <https://doi.org/10.1002/2015JA021525>
- Paulino, I., Medeiros, A. F., Vadas, S. L., Wrasse, C. M., Takahashi, H., Buriti, R. A., et al. (2016). Periodic waves in the lower thermosphere observed by OI 630 nm airglow images. *Annales Geophysicae*, 34(2), 293–301. <https://doi.org/10.5194/angeo-34-293-2016>
- Pimenta, A. A., Amorim, D. C. M., & Candido, C. M. N. (2008). Thermospheric dark band structures at low latitudes in the southern hemisphere under different solar activity conditions: A study using OI 630 nm emission all-sky images. *Geophysical Research Letters*, 35, L16103. <https://doi.org/10.1029/2008GL034904>
- Saito, A., Fukao, S., & Miyazaki, S. (1998). High resolution mapping of TEC perturbations with the GSI GPS network over Japan. *Geophysical Research Letters*, 25, 3079–3082.
- Saito, S., Yamamoto, M., Hashiguchi, H., Maegawa, A., & Saito, A. (2007). Observational evidence of coupling between quasi-periodic echoes and medium scale traveling ionospheric disturbances. *Annales Geophysicae*, 25(10), 2185–2194. <https://doi.org/10.5194/angeo-25-2185-2007>
- Sobral, J., Takahashi, H., Abdu, M., Taylor, M., Sawant, H., Santana, D. C., et al. (2001). Thermospheric F-region travelling disturbances detected at low latitude by an OI 630 nm digital imager system. *Advances in Space Research*, 27, 1201–1206. [https://doi.org/10.1016/S0273-1177\(01\)00198-3](https://doi.org/10.1016/S0273-1177(01)00198-3)
- Spilker, J. J., & Parkinson, B. W. (1996). Overview of GPS operation and design. In *Global positioning system: Theory and applications* (Vol. 1, pp. 29–56). Reston, Va: Am. Inst. of Aeronaut. and Astronaut. <https://doi.org/10.2514/5.9781600866388.0029.0055>
- Takeo, D., Shiokawa, K., Fujinami, H., Otsuka, Y., Matsuda, T. S., Ejiri, M. K., et al. (2017). Sixteen year variation of horizontal phase velocity and propagation direction of mesospheric and thermospheric waves in airglow images at Shigaraki, Japan. *Journal of Geophysical Research: Space Physics*, 122, 8770–8780. <https://doi.org/10.1002/2017JA023919>
- Taylor, M. J., Pautet, P. D., Medeiros, A. F., Buriti, R., Fehchine, J., Fritts, D. C., et al. (2009). Characteristics of mesospheric gravity waves near the magnetic equator, Brazil, during the SpreadFEx campaign. *Annales Geophysicae*, 27(2), 461–472. <https://doi.org/10.5194/angeo-27-461-2009>
- Tsugawa, T., Otsuka, Y., Coster, A. J., & Saito, A. (2007). Medium-scale traveling ionospheric disturbances detected with dense and wide TEC maps over north America. *Geophysical Research Letters*, 34, L22101. <https://doi.org/10.1029/2007GL031663>
- Vadas, S. L. (2007). Horizontal and vertical propagation and dissipation of gravity waves in the thermosphere from lower atmospheric and thermospheric sources. *Journal of Geophysical Research*, 112, A06305. <https://doi.org/10.1029/2006JA011845>
- Vadas, S. L., & Crowley, G. (2010). Sources of the traveling ionospheric disturbances observed by the ionospheric TIDBIT sounder near Wallops Island on 30 October 2007. *Journal of Geophysical Research*, 115, A07324. <https://doi.org/10.1029/2009JA015053>
- Vadas, S. L., & Fritts, D. C. (2005). Thermospheric responses to gravity waves: Influences of increasing viscosity and thermal diffusivity. *Journal of Geophysical Research*, 110, D15103. <https://doi.org/10.1029/2004JD005574>
- Valladares, C. E., & Sheehan, R. (2016). Observations of conjugate MSTIDs using networks of GPS receivers in the American sector. *Radio Science*, 51, 1470–1488. <https://doi.org/10.1002/2016RS005967>
- Zhang, F. (2004). Generation of mesoscale gravity waves in upper-tropospheric jet-front systems. *Journal of Atmospheric Sciences*, 61, 440–457. [https://doi.org/10.1175/1520469\(2004\)061<0440:GOMGWl>2.0;2](https://doi.org/10.1175/1520469(2004)061<0440:GOMGWl>2.0;2)